ARTICLE

Strength Improvement via Coating of a Cylindrical Hole by Layer-by-Layer Assembled Polymer Particles

Shuqing Wu,[‡,†] Lucas B. Garfield,[†] Nicholas E. Rupert,[†] Brian P. Grady,*[,†] and Gary P. Funkhouser[§]

School of Chemical, Biological and Materials Engineering, University of Oklahoma, Norman, Oklahoma 73019, and Halliburton Inc., Duncan, Oklahoma 73536

ABSTRACT Negatively charged colloidal poly(methyl methacrylate-*co*-butyl acrylate) (P(MMA-BA)) particles and positively charged dissolved poly(ethyleneimine) (PEI) were adsorbed onto a cement block using a layer-by-layer (LBL) assembly technique. The block was fashioned so as to have a cylindrical hole running from one face to another along the long axis of the rectangular block, and a fluid containing either of the two charged materials was pumped through the block. The result was a film tens of micrometers thick, and the pressure required to crack the cement block was measured after one end of the hole was sealed. Latex particles with a T_g near the use temperature showed the maximum improvement in the cracking stress of the blocks. In a multilayer coating with identically sized particles, the cracking stress of the blocks increased to an improvement of 25% and then dropped off with increasing number of layers, even though the relationship between film thickness and the number of layers was linear. An improvement of about 30% in the cracking stress of the coated blocks was obtained when using multiple layers with different particle sizes. The effects of the number of layers and particle size on the cracking stress suggest that both the morphology and the thickness of the film play a role in performance. Tests done under confinement, e.g., with an external stress applied to the outside of the blocks, suggest that not only does a film-forming mechanism contribute to performance but that filling of microcracks in the rock may also play a role.

KEYWORDS: layer-by-layer assembly • latex particles • poly(ethyleneimine) • mechanical properties • reservoir engineering

INTRODUCTION

The layer-by-layer assembly technique (LBL) has been widely used to create highly functional materials with nano or micrometer levels of structure via alternating adsorption of positively and negatively charged species from solutions (1–3). A broad range of materials are used in this simple and versatile approach, such as polyelectrolytes, nanoparticles, lipids and proteins. Ordered two- and three-dimensional structures can be created using driving forces such as electrostatic interactions, van der Waals forces, capillary forces, hydrogen bonding, hydrophobic interaction, etc., on various substrates, which include quartz, silicon, and metal electrodes (4, 5). LBL techniques can be categorized as one of two types: (1) those that involve adsorption of dissolved molecules (6, 7); and (2) those that involve adsorption of colloidal particles (8–10). The latter can be used to create ordered two-dimensional (2D) or three-dimensional (3D) crystalline structures (11–13). Much of the work in the LBL area focuses on the optimization of the absorption conditions; observation of morphologies; and response to optical, electrical, or other types of signals (14–17).

Recently, one area of interest for the LBL technique is the construction of nanoscopically layered materials which allow the transfer of the exceptional mechanical properties of nanoscale materials to the LBL film. Through fine control of the structure and composition of the LBL film, the mechanical properties of these multilayer composites can be improved. To improve the mechanical properties, wear, and/or friction coefficient of the adsorbed film, particles such as single-walled nanotubes (SWNT) (18–21), clay platelets (22, 23), and inorganic nanoparticles (24, 25) have been used in conjunction with molecules adsorbed from solution. The inorganic materials act as a reinforcing filler much like in traditional composites. The carefully designed structure and carefully controlled interface of dissolved polymers and nanoparticles can greatly improve the mechanical properties of thin nanocomposite films as a result of efficient stress transfer.

Although the mechanical properties of adsorbed LBL films have been the subject of a number of studies (18–25), few studies have been reported concerning how LBL adsorption affects the mechanical properties of the underlying substrate. To the best of our knowledge, only one study has reported how LBL films increase the mechanical properties of the substrate. Specifically, an LBL film was shown to increase the failure strain of polyethylene terephthalate (PET) vascular threads and prostheses by an alternating deposition

* To whom correspondence should be addressed. E-mail: bpgrady@ou.edu. Tel: (405) 325-4369. Fax: (405) 325-5813.
Received for review January 20, 2010 and accepted March 18, 2010
† University of Oklahoma.
‡ Current address: School of Materials Science and Engineering, South China University of Technology, Guangzhou 510640, China.
§ Halliburton Inc.
DOI: 10.1021/am1000618

Published on Web 03/30/2010

of polyelectrolyte film (26). The rupture limit of the coated PET threads was enhanced by more than 20% compared to uncoated threads. The mechanical property of interest in our study involved the pressurization of a fluid within a cement block which caused the expansion of microcracks, eventually leading to macroscopic cracking and failure of the block. This situation is extremely relevant to cracking of nonporous rocks, particularly shale, in oil-drilling operations. Pressurization of the rock occurs because of a combination of hydrostatic head pressure and friction pressure. Unlike our situation, where a crack leads to failure, macroscopic cracks in a borehole lead to undesirable fluid loss into the surroundings. The hypothesis being tested in this work is whether a barrier that can easily be remotely deposited is able to raise the cracking stress of rock.

The basis for making a hypothesis that a film might be able to delay the cracking stress is found in fracture mechanics. For a rectangular plate with dimensions a and b rigidly clamped at the edges, the bending moments (M_x and M_y) under a uniform pressure P_0 are as follows (27)

$$M_x = \frac{1}{12}P_0\frac{a^2b^4}{a^4 + b^4} \quad M_y = \frac{1}{12}P_0\frac{a^4b^2}{a^4 + b^4} \tag{1}$$

in the case where $b \gg a$, which is likely the case in our situation based on observed fracture patterns, the two moments simplify to

$$M_x = \frac{1}{12}P_0a^2 \quad M_y = \frac{1}{12}P_0a^2\left(\frac{a}{b}\right)^2 \tag{2}$$

Only the first equation is relevant if $b \gg a$. The relationship between stress and moment is given by (28)

$$\sigma_x = \frac{12M_xz}{t^3} \tag{3}$$

where t is the thickness of the plate and z is the distance along the z axis. The maximum stress occurs on the bottom and top surface (at $z = \pm t/2$) of the plate. Substituting M_x into eqs 3, we find that

$$\sigma_{max} = 0.5P_0(a/t)^2 \tag{4}$$

This calculation assumes no stretching at the edges of the crack (i.e., perfectly clamped edges), which means that this calculation is an overestimation of the actual stress; how much is not clear, however. This stress can be compared to a material's fracture stress to get an estimation of the ability of a material to improve the cracking stress of rock. Using reasonable estimations of a, and the tens of micrometers thicknesses measured in this paper suggest a polymer could increase the cracking stress.

Placing a barrier on shale to prevent fluid loss is not a new concept, and studies have been described that use this strategy when cracks are already present (29–32). This project deals with the situation prior to the formation of those cracks: can a barrier be placed on the walls of a borehole to increase the pressure required to crack the rock? The key technological difficulty is finding a mechanism that allows the barrier to be placed at the walls of the borehole. Using charged dissolved or dispersed polymers to adsorb onto oppositely charged walls offers a way to control the placement of polymers downhole. The relationship between the mechanical properties of the coating and the ability to resist cracking are not clear. To simulate this process, we made blocks with boreholes with a specially formulated cement. The purpose of this work was to test how the maximum pressure, e.g., the pressure that caused cracking of the block, changed with coating characteristics. Characteristics include using dissolved polymer vs colloidal particles, colloidal particle size, and polymer stiffness.

EXPERIMENTAL SECTION

Materials. Reagent-grade methyl methacrylate (MMA) and *n*-butyl acrylate (BA) monomers (purchased from Sigma-Aldrich) were passed through columns filled with inhibitor-removal packing material (from Sigma-Aldrich). Reagent-grade surfactants and initiators, sodium dodecyl sulfate (SDS, from Sigma-Aldrich), hexadecyltrimethylammonium bromide (CTAB, from Sigma-Aldrich), 2,2′-azobisisobutyronitrile (AIBN, from Sigma-Aldrich), potassium peroxodisulfate (KPS, from Fluka) and 2,2′-azobis(2-methylpropionamidine) dihydrochloride (Wako V-50, from Sigma-Aldrich) were used as received without further purification. Branched poly(ethyleneimine) (PEI, $M_w = 25\,000$) was purchased from Sigma-Aldrich. Hydromite (a resin-modified gypsum cement), Hydro-Stone (gypsum cement), and CAT-A (the catalyst for the resin-modified gypsum cement) were purchased from United States Gypsum Company, Chicago, Illinois. CFR-3 (a sulfonated resin cement dispersant) was provided by Halliburton Inc., Duncan, Oklahoma.

Synthesis of Latex. Latex synthesis was performed in a 2 L four-necked reaction flask equipped with a reflux condenser, a nitrogen gas inlet, a mechanical stirrer, and a feed tube for monomer, surfactant, and initiator.Nine-hundred milliliters of deionized water was added to the flask. Nitrogen was bubbled through the water for 30 min and then a nitrogen blanket was used for the duration of the reaction. Surfactant was then added and stirred for 0.5 h. A prewashed comonomer mixture (the fraction of the MMA and BA was adjusted according to the desired T_g) was added and allowed to mix for 1 h to equilibrate. Initiator was added to the mixture, and the reaction mixture was raised to 70 °C and then stirred overnight. The latex was cooled to room temperature and filtered. The procedure for emulsifier-free emulsion polymerization was the same, except no surfactant was used and the stirring speed was much more vigorous. KPS and V-50 were used as initiators in the emulsifier-free emulsion polymerization. SDS and CTAB were used as surfactants in the emulsion polymerization to make the latex particles negatively or positively charged, respectively. The surface charge of the latex particles in the emulsifier-free emulsion polymerization is due to bonded sulfate ions ($-OSO_3^-$) and protonated-amidine ions contributed by KPS or V-50, respectively (33). In all cases, a visually homogeneous dispersed material was the result. Particle size and zeta potential of the particles were measured with a Brookhaven 90Plus/BI-MAS particle size analyzer and ZetaPlus zeta potential analyzer (Brookhaven Instruments Corporation, Holtsville, NY), respectively, at 25 °C. A TA Instruments Q-1000 differential scanning calorimeter (DSC, TA Instruments Corporation, New Castle, DE) was used for glass-transition temperature determination at a

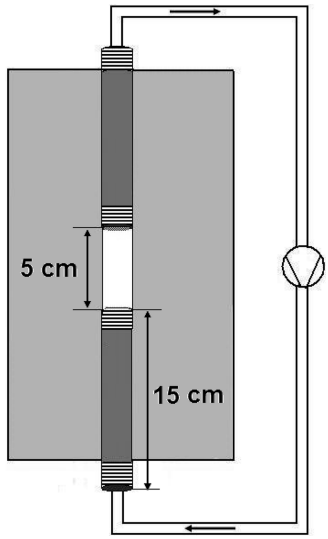

FIGURE 1. Schematic of setup for the coating process. For testing, the line from the block to the suction side of the pump was disconnected and that side of the pipe was capped.

heating rate of 10 °C/min after fully drying and then melting the latex in a DSC pan.

Fabrication of Testing Blocks. The testing block was a rectangular block with approximate dimensions 22.9 cm ×15.2 cm ×15.2 cm ($H \times W \times L$). In the center, along the long axis of the block, two 1/2 in. nominal steel pipes (2.1 cm OD) with threads at both ends were inserted. They were inserted so that at each face one set of threads was exposed. Internally they were separated by an approximately 5.0 cm gap, kept open by inserting a metal cylinder with tightly fitting poly(vinyl chloride) (PVC) braided tubing over it. The PVC tubing was threaded through both steel pipes before cement was poured into the mold. The metal cylinder and PVC tubing were sized so that the tubing with the cylinder inside could be removed after the cement hardened around the pipes. In other words, the opening was slightly smaller than the 1.6 cm steel pipe ID. A schematic of the finished block is shown in Figure 1. The result was a block with a hole all the way through with a ~5 cm region in the middle open to cement.

A number of different block formulations were tested. The key performance parameter was to produce a hydrophilic surface impermeable to water on the experimental time and pressure scale. Formulations based solely on gypsum cement, water, and dispersant were too permeable to develop sufficient pressure to crack the block within the flow-rate range of the hydraulic pump. The material with the composition below was hydrophilic (as indicated by the fact that water droplets spread on the surface) and had sufficiently low permeability.

The final block formulation was:

- 28% Hydromite (plus 1% CAT-A based on the amount of Hydromite)
- 72% Hydro-Stone (plus 2% CFR-3 based on the amount of Hydro-Stone)
- 26 parts water (based on 100 parts of solids)

CFR-3 was dissolved in the water. All other components were mixed together; these components were all powders. The water-CFR-3 solution was poured into the powder mixture. The mixture was mixed by hand until homogeneous. The slurry was then poured into a mold to form a block. All of the blocks were aged in air for more than 2 weeks. A small amount of slurry was poured onto a piece of plastic film to a thickness of roughly 1.5 mm, and then dried in air. The cement piece was broken into small chips which were used in the measurement of samples via scanning electron microscopy.

Fabrication of Coating Film and Cracking Stress Measurement. The inner surfaces of the blocks were pretreated with 1% PEI or 1% $CaCl_2$ aqueous solution for 1 h in order to promote the adhesion of a negatively charged latex to the block surface. Negatively charged latex (10% dispersion) was pumped through the block against the pull of gravity at 600 mL/min (velocity =5 cm/s) for 12 min. Blocks were then rinsed with DI water to remove weakly bound particles in order to avoid their aggregation and plug formation when PEI solution or oppositely charged latex was pumped through during the next adsorption step. The procedure was repeated until the desired number of layers was obtained and the blocks were rinsed with DI water after each deposition step (pH value of the water used in this work was measured as 5.38). There was minimal change in latex concentration during the coating process; however, the zeta potential did change somewhat, so the latex was discarded after 3−5 coatings.

Once all layers had been coated, the block was tested at room temperature without drying. One opening was sealed by screwing a cap onto the threads and the other was connected to a Ruska hydraulic pump (Ruska Instruments Corporation, Houston, TX). The stress was measured at a pump speed corresponding to a water flow rate of 50 mL/min until the blocks were broken. This speed corresponded to an increase in pressure of 7 MPa (1000 psi) in ~5 s. The cracking stress was taken as the maximum stress, and averages of five to ten measurements are reported. Roughly 20% of the blocks tested had failure stresses far below that of the other 80%, which was attributed to imperfections in the block manufacture since blocks with no coatings had this error rate as well. These values were not included in the averages.

Scanning Electron Microscopy (SEM). A thin chip obtained as described above was mounted in a tube with approximately the same diameter as the diameter of the cylindrical hole of the block and treated in the same manner as the block prior to testing for the cracking stress. Coated chips were dried in air, and the cross-section morphologies of the layers were imaged with JEOL JSM 880 field-emission scanning electron microscope after being freeze fractured and sputter-coated. A high T_g (75 °C) latex was used so as to minimize sphere deformation during sample preparation and imaging.

Mechanical Property Tests. Latex solution was left to evaporate at room temperature, fully dried in a vacuum oven overnight, and then compression molded into films. Tensile tests were performed using a United STM-2K tensile tester (United Calibration Corporation, Huntington Beach, CA) with ASTM D-1708 dog-bones at 10 mm/min. For accuracy, the measurement was reproduced and averaged from 5 samples.

RESULTS AND DISCUSSION

Synthesis and Characterization of P(MMA-BA) Latex. MMA and BA were selected as the comonomers because the T_g of the copolymer (and hence the polymer stiffness) can be easily changed over a large temperature range by using different monomer feed ratios. T_g values of BA and MMA homopolymers are −49 and 105 °C, respectively (34). The monomer ratio used in the feeding stage was calculated with the Pochan equation (35)

$$\ln T_g = M_1 \ln T_{g1} + M_2 \ln T_{g2} \qquad (5)$$

where M_1 and M_2 are the mass fractions of the monomers in the feeding, and T_{g1} and T_{g2} (K) are the glass transition temperatures of the homopolymers of the monomers. A broad glass transition on the order of 40 °C was found in

Table 1. Effect of Pretreatment on Cracking Stress of One Layer Coating[a]

pretreatment	particle size (nm)	zeta potential (mv)	T_g (°C)	cracking stress (MPa)
bare surface				7.36 ± 0.18
$CaCl_2$	116.3 ± 2.2	−(34.72 ± 4.71)	40.4	7.96 ± 0.24
PEI	116.3 ± 2.2	−(34.72 ± 4.71)	40.4	8.27 ± 0.19

[a] The coating flow rate is 2500 mL/min.

DSC measurements for all of the synthesized copolymers, indicating that there was some compositional heterogeneity within the copolymer. T_g values tested by DSC were consistently 10−20 °C higher than calculated from the Pochan equation (data not shown).

Effect of Pretreatment Layer and Coating Flow Rate. Results in Table 1 show that the cracking stress of the blocks was increased by a one-layer latex coating after pretreatment with either PEI or $CaCl_2$ solution. The improvement of blocks pretreated with PEI solution is almost 0.3 MPa higher than those pretreated with $CaCl_2$. Using the student t-test, the two were statistically different at an ~98% confidence interval. SEM images show that the thickness of the coating after pretreatment with PEI (Figure 2a) is almost two times that of the coating after pretreatment with $CaCl_2$ (Figure 2b). Cracks in the films shown in SEM images were almost certainly caused by stresses releasing during the drying process (36).

During $CaCl_2$ soaking, metal cations are expected to readily adsorb onto the block surface, leaching out anions, and making the surface more positive. However, Ca^{2+} ions could only adsorb at single sites. Branched PEI is a weak polybase containing primary, secondary, and tertiary amine groups. At pH values below 6, it is highly ionized and behaves as a moderately charged cationic polyelectrolyte (37). The potential is as high as +90 mV at a higher bulk concentration (38). PEI can adsorb onto block surfaces at multiple sites due to its polymeric nature. Such multiple-"anchored" polymers would have a more stable adsorption and higher charge density on the block surface than a single Ca^{2+} cation (39). Hence, PEI has more stable adsorption on the block surface, higher charge density, and stronger adhesion to the oppositely charged latex particles. It is difficult to understand why, even with multiple site adsorption or high charge density, the thickness of a one-layer film is 60 μm (e.g., a layer thickness of approximately 600 particles). Also difficult to understand is why, with $CaCl_2$ soaking only, does a 30 μm film (e.g., 300 particles) result. In other words, the growth mechanism that enables such thick films is not clear. Elbert (40), Picart (41), DeLongchamp (42), Schoeler (43), and their co-workers found both the mass and the thickness of the film increased exponentially with the number of deposition steps when polycations and polyanions were alternately deposited on solid surfaces. Picart (44) and Lavalle (45) suggested that this growth resulted from an "in" and "out" diffusion of the diffusing species of the two polyelectrolytes constituting the films during buildup. The diffusing specie diffuses throughout the film down into the substrate and out of the film as the procedure changed. As the diffusing species reaches the outer layer of the film, it interacts with the incoming countercharged polyelectrolyte, forming a new layer. This mechanism certainly could be playing a role, especially in the case of PEI layers. As latex particles adsorb onto PEI film, some PEI adsorb to the latex particles while a fraction of PEI molecules diffuse toward the outer layer of the film forming a new outer PEI/particle layer. The overall thickness of the layer is proportional to the amount of PEI that diffuses out of the film during the buildup step (Figure 2c).

A number of methods have been used to produce 3D colloidal arrays from monodisperse colloidal dispersions. For example, in a popular gravity sedimentation process, highly ordered arrays can be generated with thicknesses from tens of micrometers to 1 mm (46, 47). The use of evaporating water can be used to form thick layers on vertically oriented surfaces as demonstrated in one recent paper. In this case, the liquid level decreases as given by an evaporation rate, and thicker films result if the evaporation rate is very slow. With replenishment possible from the bulk solution with a slow evaporation rate, the maximum thickness has been found to be up to 120 μm (48). In our case, substrates were vertical and no gravity sedimentation should occur. We believe that there is no substantial increase or decrease in the thickness of the film after placement because water is used to flush the system after the liquid is drained and the blocks were tested without drying. Two papers that might have bearing on our situation involve a rocking sample which deposits colloids via gravity sedimentation. As a result, the amount of shear varies throughout the cell leading to various crystalline structures in different regions of the sample (49, 50). Well-stacked 3D colloidal arrays were formed by shear forces, and the thicknesses were reported from 10 to 115 μm (49). In our case, perhaps capillary forces due to the very thin water film on inner latex layers or shear forces due to different water flow rates among the different particle layers may play roles in the stacking of particles. It should be noted, however, that even in the case of no flow rate, the films were also quite thick.

Different volumetric flow rates, 0, 600, and 2500 mL/min, were tested. Blocks were pretreated for 1 h with 1% PEI solution, and then negatively charged latex was pumped (or allowed to sit for the 0 mL/min) through the hole at a contact time of 12 min. The results (Table 2) show that coating flow rate has little or no effect on the performance of the coating as a barrier to pressure-induced cracking.

Effect of Particle Stiffness. The stiffness of particles would likely have a significant effect on the ability of a layer of particles to act as a barrier against pressure-induced cracking. The temperature dependence of the particle stiffness is extremely important for downhole operations, because the temperature is much higher than atmospheric temperature and the temperature varies depending on location. The temperature dependence of the particle stiffness is strongly correlated with the glass transition temperature and hence composition. As described earlier, polymers with different T_g values and hence different Young's moduli

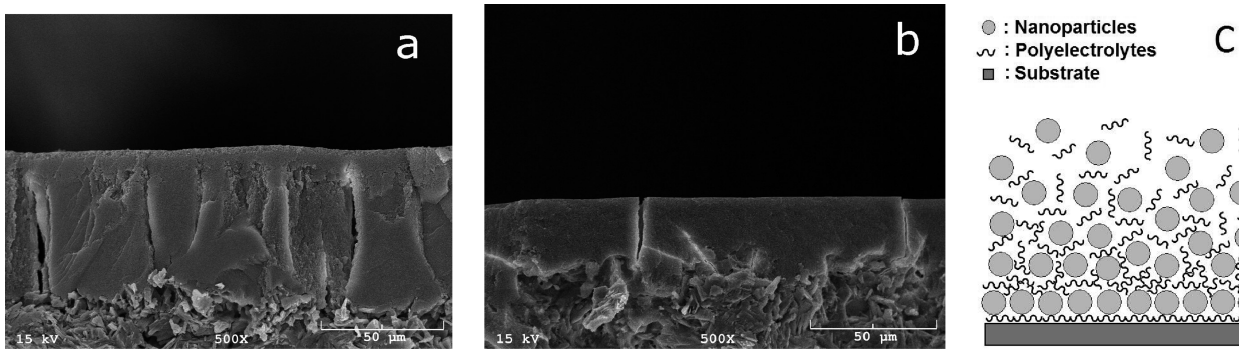

FIGURE 2. SEM images of one-layer coating: (a) treated with 1% PEI aqueous solution, (b) treated with 1% $CaCl_2$ aqueous solution, (c) schematic graph of the adsorption.

Table 2. Effect on the Cracking Stress of Coating Flow Rate

flow rate (mL/min)	particle size (nm)	zeta potential (mv)	T_g (°C)	cracking stress (MPa)
0	110.4 ± 0.8	−(41.04 ± 1.21)	21	8.70 ± 0.32
600	100.9 ± 1.1	−(46.78 ± 1.14)	20	8.66 ± 0.29
2500	127.0 ± 0.6	−(47.02 ± 0.02)	17	8.56 ± 0.15

Table 3. T_g and Mechanical Properties of P(MMA-BA)

T_g (°C)	modulus (MPa)	stress at break (MPa)	strain at break (%)
75	799.5	46.4	6.5
40	345.4	15.5	234
20	9.9	2.3	209

at room temperature were obtained by using emulsifier-free polymerization with different monomer feed ratios as shown in Table 3. Emulsifier-free polymer was used to avoid the plasticizer effect of surfactants in tensile tests. Average values of tensile properties are shown in Table 3. Materials with T_g values less than 20 °C could not be measured, as samples could not be loaded in the testing machine because of insufficient stiffness.

The relationship between average cracking stress and T_g is shown in Figure 3. The best cracking stress was achieved when the T_g was around room temperature (20−40 °C), whether the blocks were soaked with $CaCl_2$ or PEI solution. If the T_g is lower than 0 °C or higher than ∼40 °C, the cracking stress was lower. In other words, the beads need to have some flexibility, but cannot be too flexible. This data shows that, for a one layer coating, T_g near the use temperature is the appropriate type of latex to use. The operating regime is also quite wide, it is likely that if the operation temperature is x (°C), then a particle with a T_g between ∼(x + 10 °C) ± 15 °C will give optimal performance.

The deposition process in this work can be described by the irreversible multilayer growth process (51–53). In the irreversible multilayer growth model, particles adsorb onto the tops of particles of lower layers. The particles are deposited at random, and most of the area is filled at an early stage. Some small disconnected areas form confined regions; some particles deposit and stack at the first site reached, creating "overhangs" that shadow the lower layer and leave permanent voids (Figure 4a). Figure 4b is an SEM

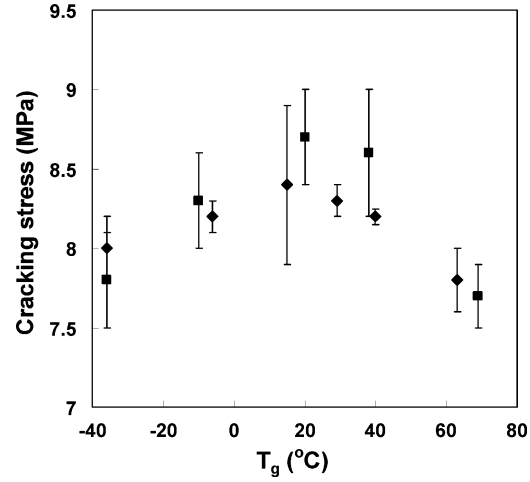

FIGURE 3. Cracking stress of one layer coating with different T_g. ■, soaked with 1% PEI water solution; ◆, soaked with 1% $CaCl_2$ water solution.

image taken of the top of a coating layer. After the chip was coated with latex particles with a T_g of 75 °C, it was lyophilized to prevent the rearrangement of the particles due to strong capillary pressures during the drying process (54). The "overhangs", voids, and confined areas on the coatings surface can be easily seen in the SEM image. If particles were able to deform somewhat, then the voids would be significantly narrowed or even closed. At a certain point, there would not be a fluid path through the particle layer to the surface and hence the layer would truly act as a barrier shield. Based on this mechanism, higher T_g (>40 °C) latex particles should show a lower cracking stress than those with a medium T_g (20−40 °C) because the higher T_g particles are harder to deform. Although the lower T_g (<0 °C) latex particles can deform much more easily to close the voids in the coating layer, experimentally they showed lower cracking stresses, likely because the film was too weak. Blocks pretreated with PEI showed higher cracking stresses than those pretreated with $CaCl_2$, which is logical because of the fact that the former pretreatment yields a thicker layer.

Effect of Number of Layers. The differences between blocks coated with PEI as the initial pretreatment layer and those coated with $CaCl_2$ suggest that the thickness plays an important role in determining performance. Hence, blocks were coated with 1, 3, 5, and 7 layers of negatively charged latex with a $T_g \approx 20$ °C. To adsorb different

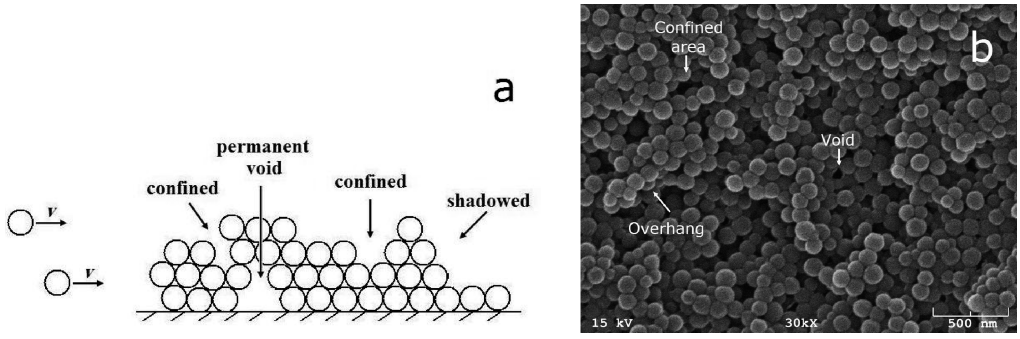

FIGURE 4. (a) Schematic of the multilayer growth process, and (b) SEM image of the coatings morphology

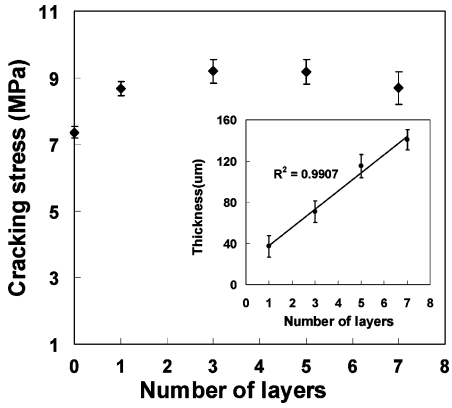

FIGURE 5. Effect of number of layers on the cracking stress. Inset shows a linear increase in thickness with number of layers.

numbers of layers, PEI was used as the positively charged layer. Also, as noted in the Experimental Section, in all cases the contact time for an individual layer was 12 min and water was pumped through the system between the deposition of negative and positive layers to prevent plugging of the pump.

The results of the cracking stress experiments are shown in Figure 5. According to the t test, the cracking stress of 1 and 3 layers was statistically different at a 94% confidence interval. The cracking stress of 3 and 5 layers was statistically identical at a 93% confidence interval. This result indicates that, as expected, the performance increases as the number of layers increase, and eventually reaches a plateau. Much more surprising is that for 5 and 7 layers, the two results were statistically different at a 97% confidence level. Hence, there seems to be an optimal number of layers, i.e., the cracking stress decreases if the number of layers is too large. The only reasonable explanation is that the reduction is due to defects in the coating layers accumulating with additional layers.

After testing, blocks were broken with a hammer after air drying, coatings were peeled off, and film thicknesses were measured with calipers. The films were homogeneous, free-standing, semitransparent, and flexible. It should be noted that we do NOT believe that these are the characteristics of the film prior to drying. Because of the flexibility of the particles due to the low T_g, particles were deformed elastically and the interparticle voids were closed under the high capillary pressures caused by the free water evaporation from the surface during the drying process (55). However, film thickness as measured by this technique should provide a relative measure of the films thickness during testing. The inset of Figure 5 shows that the thickness increased linearly with the number of coating layers, indicating that the cracking stress results were not the result of some unexpected thickness behavior.

Table 4. Comparison of Cracking Stress of Multilayers with Same and Different T_g Values

	cracking stress (MPa)	
layers (in total)	same T_g	different T_g
3	8.92 ± 0.45	9.17 ± 0.41
5	8.72 ± 0.27	8.54 ± 0.34

Multiple layers offer the opportunity to have a film with different stiffness as a function of thickness. For these experiments, instead of using multiple layers of negatively charged latex separated by a polyelectrolyte, we used positively charged latex to build up a coating with latices of different T_g values in layers. Nanoparticles of identical size (~120 nm) and different T_g values (20 and 70 °C) were used to create the alternating negatively and positively charged layers (Table 4). So, for example, for the 5-layer data with different T_g values shown in Table 4, from the surface of the block the layers were arranged according to the following: soft (negative)—hard (positive)—soft (negative)—hard (positive)—soft (negative). For comparison, a coating with particles of the optimal stiffness (e.g., T_g near room temperature) was also built in a similar manner and tested.

The results are statistically different at a ~58% confidence interval for both 3 layers and 5 layers, respectively. Because these numbers are not very high, we are safe in saying that alternating the stiffness of the various layers did not significantly improve results.

Effect of Particle Size. Visual examination of Figure 4 suggests that a film with lower porosity might be obtained if layers of differently sized particles were constructed. The cracking stress did not change significantly by varying the particle size of a single layer of negatively charged latex adsorbed onto PEI (Table 5). Under perfect packing with monodisperse spheres, the porosity of the film would be the same, so perhaps this result is not surprising. However, it should also be noted that although unmeasured, the thickness of the layers with larger particles is expected to be higher.

Table 5. Cracking Stress of a Single Layer with Different Particle Size

particle size (nm)	zeta potential (mv)	T_g (°C)	cracking stress (MPa)
100.9 ± 1.1	−(46.78 ± 1.14)	20	8.66 ± 0.29
556.4 ± 30.7	−(49.33 ± 1.07)	21	8.54 ± 0.53
803.4 ± 10.5	−(64.86 ± 1.43)	22	8.65 ± 0.58

Table 6. Cracking Stress of a Five-Layer Coating with Different Size Particles[a] in Positively Charged Layers

runs	particle size (nm)	zeta potential (mv)	film thickness[b] (μm)	cracking stress (MPa)
1	116.8 ± 0.4	−(31.99 ± 0.6)	57.6 ± 8.3	8.72 ± 0.27
	126.3 ± 1.7	43.66 ± 0.8		
2	119.1 ± 1.5	−(35.10 ± 5.02)	194.2 ± 12.2	9.52 ± 0.67
	502.1 ± 17.3	52.84 ± 3.44		
3	119.2 ± 0.9	−(41.04 ± 1.21)	172.8 ± 16.7	9.14 ± 0.23
	1062.7 ± 30.3	42.04 ± 0.7		

[a] T_g values of all of particles are ~20 °C. [b] Thickness in dry state.

A more interesting experiment using multilayers is to change the particle size of the positively charged layers, for example, in a five layer experiment the sizes were: small (negative)−large (positive)−small (negative)−large (positive)−small (negative). Results are shown in Table 6.

The film thickness of layers constructed from identically sized particles built via latex and PEI in Figure 5 is about twice as high as those built with the same number of particulate layers but with alternating negative and positive particles, as shown in Table 6 (i.e., 115.1 μm vs 57.6 μm). Such a difference cannot be explained by the thickness of five discrete PEI layers; however, diffusion and interpenetration of PEI in the coating process could explain this difference. Comparing results shown in Table 6, the film thickness with 500 nm positively charged particles is 3.4 times that of the film with 120 nm positively charged particles, which is much larger than the calculated value of 2.3 based on the diameter ratio and number of layers. Also, the layer thickness is smaller with 1000 nm positively charged particles than with 500 nm particles. We do not have an explanation for either result.

Cracking stress results shown for the layer containing 500 nm particles were the highest achieved, likely indicating that using smaller particles to help fill the void volume of larger particles is a mechanism that increases the cracking stress. Quantitatively, a 5-layer coating made with latex and PEI (thickness =115.1 μm) gave a maximum increase of ~25% in cracking stress (Figure 5), whereas the same number of particulate layers but with different charges (thickness =57.6 μm) gave an increase of ~20%; with both varying charges and particle size (thickness =194.2 μm), the improvement increased to ~30%. This data indicates that both morphology and thickness determine the effectiveness of a particular film with respect to increasing cracking stress.

Confinement Experiments. One significant difference between our experiments and conditions downhole is that downhole rocks are under a great deal of confining stress. In order to simulate downhole conditions, confining stresses of 2.0, 1.4, and 0.7 MPa in the z, x, and y axis directions, respectively, were applied to a block after it was pretreated with PEI, then the block was in situ coated (i.e., after the confining stress was applied) with one layer of latex and the cracking stress was measured. All other variables were the same as in the unconfined tests. The results with and without confinement are shown in Table 7.

Table 7. Cracking Stress with and without Confinement

	cracking stress (MPa)		
test	no coating	after coating	improvement (MPa)
unconfined	7.36 ± 0.18	8.66 ± 0.29	1.30
confined	6.87 ± 0.48	8.16 ± 0.36	1.29

Table 8. Cracking Stress of Off-Line and In situ Coating with Confinement

coating	particle size (nm)	zeta potential (mv)	T_g (°C)	cracking stress[a] (MPa)
off-line	126.4 ± 1.3	−(41.08 ± 1.68)	16	7.15 ± 0.14
in situ	128.1 ± 1.0	−(54.43 ± 1.04)	20	7.81 ± 0.59

[a] The testing pressure went up to 5.5 MPa first and then increased at 1.0 MPa/min until the blocks were broken.

Within statistical error, improvements are identical when identical procedures are used and blocks are coated in situ. A drop in cracking stress occurs under confinement, about 0.5 MPa, which occurs regardless of whether a coating is present or not. When the coating was first applied with no confining pressure, then the confining pressure was added and the cracking stress tested (a situation we have termed off-line coating), a much smaller improvement in the cracking stress occurred, as shown in Table 8.

Our belief is that the difference in cracking stress shown in Table 8 between off-line and in situ coated blocks was due to either one or both of two factors. First, when confinement pressures were applied to blocks coated off-line, openings (or defects) may have occurred in the coating layer during the application of the confining pressure. However, it is difficult to understand why a fairly flexible film would lead to the formation of cracks during confinement. Such a response would be more understandable if an extensional load were applied; however, given the small strains that the rock would experience even in tension, cracks would be hard to understand. Second, microcracks in the rock were filled by the coating layer. In the in situ case, the microcracks were still properly filled after application of the stress, while in the other case, changes in the shape or size of the microcracks during application of the confining pressure could have occurred without reorganization of the coating layer to properly fill the cracks. This explanation seems reasonable and is more likely to be true than the first. Hence, these tests suggest that filling of microcracks contributes to the improvement in cracking stress.

CONCLUSIONS

Latex particles were assembled on the inner wall of cement blocks using layer-by-layer assembly. The cracking

stress of the blocks was evaluated as a function of the characteristics of the latex film. The effects on the cracking stress of particle glass transition temperature, particle size, composition of the LBL layer, and the thickness of the film were investigated. Latex particles with a T_g of around use temperature gave the greatest improvement in performance, indicating that beads with some flexibility were necessary, but too much flexibility led to a weak film. The best result, an improvement of about 30% (2.2 MPa) in the cracking stress of the coated blocks, was obtained when using layers with different particle sizes. Using identically sized spheres, the strength of the blocks increased to a plateau of improvement of 25% and then dropped off with increasing film thickness. The effect of the number of layers and particle size suggests that both the morphology and the film thickness play a role in performance. Confinement tests suggest that not only does a film-forming mechanism contribute to performance, but that filling of microcracks in the rock may also play a role.

Acknowledgment. This work was financially supported by Halliburton Inc. We gratefully acknowledge Mr. David Meadows of Halliburton Inc. for his help in confinement experiments. We thank Dr. Preston Larson and the OU Noble Microscopy Lab for the SEM images shown in this paper.

REFERENCES AND NOTES

(1) Wang, Y. J.; Angelatos, A. S.; Caruso, F. *Chem. Mater.* **2008**, *20*, 848–858.
(2) Decher, G. *Science* **1997**, *277*, 1232–1237.
(3) Peyratout, C. S.; Dahne, L. *Angew. Chem., Int. Ed.* **2004**, *43*, 3762–3783.
(4) Quinn, J. F.; Johnston, A. P. R.; Such, G. K.; Zelikin, A. N.; Caruso, F. *Chem. Soc. Rev.* **2007**, *36*, 707–718.
(5) Hammond, P. T. *Adv. Mater.* **2004**, *16*, 1271–1293.
(6) Guo, Y. M.; Geng, W.; Sun, J. Q. *Langmuir* **2009**, *25*, 1004–1010.
(7) Hyde, K.; Rusa, M.; Hinestroza, J. *Nanotechnology* **2005**, *16*, 422–428.
(8) Priya, D. N.; Modak, J. M.; Raichur, A. M. *ACS Appl. Mater. Interfaces* **2009**, *1*, 2684–2693.
(9) Crespilho, F. N.; Zucolotto, V.; Brett, C. M. A.; Oliveira, O. N., Jr.; Nart, F. C. *J. Phys. Chem. B* **2006**, *110*, 17478–17483.
(10) Srivastava, S.; Kotov, N. A. *Acc. Chem. Res.* **2008**, *41*, 1831–1841.
(11) Goldenberg, L. M.; Jung, B. D.; Wagner, J.; Stumpe, J.; Paulke, B. R.; Goernitz, E. *Langmuir* **2003**, *19*, 205–207.
(12) Li, W.; Yang, B.; Wang, D. Y. *Langmuir* **2008**, *24*, 13772–13775.
(13) Ren, Z. Y.; Zhang, X. M.; Zhang, J. H.; Li, X.; Pan, X. Q.; Fei, X.; Cui, Z. C.; Yang, B. *J. Mater. Chem.* **2008**, *18*, 3536–3538.
(14) Oliveira, O. N., Jr.; He, J. A.; Zucolotto, V.; Balasubramanian, S.; Li, L.; Nalwa, H. S.; Kumar, J.; Tripathy, S. K. *Handbook of Polyelectrolytes and Their Applications*; American Scientific: Valencia, CA, 2002; Vol. 1, pp 1−37.
(15) Haberska, K.; Ruzgas, T. *Bioelectrochemistry* **2009**, *76*, 153–161.
(16) Park, H. J.; Kim, J.; Chang, J. Y.; Theato, P. *Langmuir* **2008**, *24*, 10467–10473.
(17) Meyer, S.; Pescador, P.; Donath, E. *J. Phys. Chem. C* **2008**, *112*, 1427–1434.
(18) Shim, B. S.; Zhu, J.; Jan, E.; Critchley, K.; Ho, S.; Podsiadlo, P.; Sun, K.; Kotov, N. A. *ACS Nano* **2009**, *3*, 1711–1722.
(19) Mamedov, A. A.; Kotov, N. A.; Prato, M.; Guldi, D. M.; Wicksted, J. P.; Hirsch, A. *Nat. Mater.* **2002**, *1*, 190–194.
(20) Tang, Z. Y.; Kotov, N. A.; Magonov, S.; Ozturk, B. *Nat. Mater.* **2003**, *2*, 413–418.
(21) Huang, G.; Wang, B.; Lu, H. B.; Mamedov, A.; Gupta, S. *J.Appl. Mech.* **2006**, *73*, 737–744.
(22) Podsiadlo, P.; Kaushik, A. K.; Arruda, E. M.; Waas, A. M.; Shim, B. S.; Xu, J. D.; Nandivada, H.; Pumplin, B. G.; Lahann, J.; Ramamoorthy, A.; Kotov, N. A. *Science* **2007**, *318*, 80–83.
(23) Podsiadlo, P.; Tang, Z. Y.; Shim, B. S.; Kotov, N. A. *Nano Lett.* **2007**, *7*, 1224–1231.
(24) Pavoor, P. V.; Gearing, B. P.; Gorga, R. E.; Bellare, A.; Cohen, R. E. *J. Appl. Polym. Sci.* **2004**, *92*, 439–448.
(25) Sennerfors, T.; Bogdanovic, G.; Tiberg, F. *Langmuir* **2002**, *18*, 6410–6415.
(26) Rinckenbach, S.; Hemmerle, J.; Dieval, F.; Arntz, Y.; Kretz, J.; Durand, B.; Chakfe, N.; Schaaf, P.; Voegel, J.; Vautier, D. *J. Biomed. Mater. Res., A* **2008**, *84A*, 576–588.
(27) Ugural, A. C. *Stresses in Plates and Shells*; McGraw Hill: New York, 1981; pp 80−82.
(28) Ugural, A. C. *Stresses in Plates and Shells*; McGraw Hill: New York, 1981; pp 6−9.
(29) Alford, S.; Dzialowski, A.; Jiang, P.; Ullmann, H. *SPE/IADC* **2001**, 67737.
(30) Borchardt, J. K. *Colloids Surf.* **1992**, *63*, 189–199.
(31) Schlemmer, R.; Friedheim, J. E.; Growcock, F. B.; Bloys, J. B.; Headley, J. A.; Polnaszek, S. C. *SPE Drill. Completion* **2003**, *18*, 318–331.
(32) Oort, E. V. *J. Petrol. Sci. Eng.* **2003**, *38*, 213–235.
(33) Goodall, A. R.; Wilkinson, M. C.; Hearn, J. *J. Polym. Sci.: Polym. Chem.* **1977**, *15*, 2193–2218.
(34) Brandrup, J.; Immergut, E. H.; Grulke, E. A. *Polymer Handbook*, 4th ed.; John Wiley & Sons: New York, 1999; Vol. 1, p VI/199 and VI/203.
(35) Couchman, P. R. *Macromolecules* **1978**, *11*, 1156–1161.
(36) Atkinson, A.; Guppy, R. M. *J. Mater. Sci.* **1991**, *26*, 3869–3873.
(37) Chen, K. M.; Jiang, X. P.; Kimerling, L. C.; Hammond, P. T. *Langmuir* **2000**, *16*, 7825–7834.
(38) Poptoshev, E.; Claesson, P. M. *Langmuir* **2002**, *18*, 2590–2594.
(39) Himes, R. E.; Vinson, E. F.; Simon, D. E. *SPE Prod. Eng.* **1991**, *6*, 252–258.
(40) Elbert, D. L.; Herbert, C. B.; Hubbell, J. A. *Langmuir* **1999**, *15*, 5355–5362.
(41) Picart, C.; Lavalle, P.; Hubert, P.; Cuisinier, F. J. G.; Decher, G.; Schaaf, P.; Voegel, J. C. *Langmuir* **2001**, *17*, 7414–7424.
(42) DeLongchamp, D. M.; Kastantin, M.; Hammond, P. T. *Chem. Mater.* **2003**, *15*, 1575–1586.
(43) Schoeler, B.; Poptoshev, E.; Caruso, F. *Macromolecules* **2003**, *36*, 5258–5264.
(44) Picart, C.; Mutterer, J.; Richert, L.; Luo, Y.; Prestwich, G. D.; Schaaf, P.; Voegel, J.; Lavalle, P. *Proc. Natl. Acad. Sci. U.S.A.* **2002**, *99*, 12531–12535.
(45) Lavalle, P.; Vivet, V.; Jessel, N.; Decher, G.; Voegel, J.; Mesini, P. J.; Schaaf, P. *Macromolecules* **2004**, *37*, 1159–1162.
(46) Xia, Y. N.; Gates, B.; Yin, Y. D.; Lu, Y. *Adv. Mater.* **2000**, *12*, 693–713.
(47) Kumacheva, E.; Kalinina, O.; Lilge, L. *Adv. Mater.* **1999**, *11*, 231–234.
(48) Shimmin, R. G.; DiMauro, A. J.; Braun, P. V. *Langmuir* **2006**, *22*, 6507–6513.
(49) Amos, R. M.; Rarity, J. G.; Tapster, P. R.; Shepherd, T. J.; Kitson, S. C. *Phys. Rev. E* **2000**, *61*, 2929–2935.
(50) Schoepe, H. J. *J. Phys.: Condens. Matter* **2003**, *15*, L533–L540.
(51) Evans, J. W. *Rev. Mod. Phys.* **1993**, *65*, 1281–1239.
(52) Ryde, N.; Kallay, N.; Matijevic, E. *J. Chem. Soc., Faraday Trans.* **1991**, *87*, 1377–1381.
(53) Bartelt, M. C.; Privman, V. *Phys. Rev. A* **1991**, *44*, R2227–R2230.
(54) Denkov, N.D.; Velev, O. D.; Kralchevsky, P. A.; Ivanov, I. B.; Yoshimura, H.; Nagayama, K. *Nature* **1993**, *361*, 26.
(55) Pauchard, L.; Abou, B.; Sekimoto, K. *Condensed Matter* **2009**, 1–22.

AM1000618